On the interpretation of kinetic effects from ionization in fluid models and its impact on filamentary transport

Thrysøe, A. S.; Poulsen, A. S.; Wiesenberger, M.

Published in:
Physics of Plasmas

Link to article, DOI:
10.1063/5.0122234

Publication date:
2023

Document Version
Peer reviewed version

On the interpretation of kinetic effects from ionization in fluid models and its impact on filamentary transport

A.S. Thrysøe[1]*, A.S. Poulsen[1] and M. Wiesenberger[1]

[1]PPFE, DTU Physics, Technical University of Denmark, 2800 Kgs. Lyngby, Denmark

January 3, 2023

Abstract

In regions where plasma is not fully ionized, such as the edge and scrape-off layer (SOL) regions in a tokamak, the charged particles may be subject to strong sources from interactions with neutral atoms and molecules. Such sources, e.g., from electron impact ionization, can introduce kinetic effects, as the ionized particles may have a flow velocity and temperature different from that of the main species. If treated in the conventional fluid picture, this kinetic effect emerges as a frictional heating term. In this paper the physics of this term is discussed, both for un-magnetized and magnetized plasmas. The fluid source terms are mapped back to the kinetic sources to provide a consistent picture for future model comparison. In the limits of low and high ratios between the rates of thermalization and ionization, a multi-ion species drift-fluid model is applied to assess the impact of this kinetic effect on SOL drift-plane plasma transport. This is done by modeling a seeded blob where the ions follow either a single- or double-Maxwellian velocity distribution function (VDF). It is found that the robustness of the magnetized plasma VDF in the drift-plane, and the limited effect on the vorticity source, ensure that the impact of kinetic effects on the perpendicular blob evolution is small, even in the limit of high ionization to thermalization rate ratio, where kinetic effects to the ion VDF are significant.

*Corresponding author: alec@fysik.dtu.dk

1 Introduction

In balance with the transport of particles, momentum, and heat, sources to the plasma shape magnetically confined plasmas. The profiles at the plasma edge and Scrape-Off Layer (SOL) regions determine the exhaust of particles and heat from the core and are central in regulating the machine performance [1]. The sources at the colder plasma boundary originate largely from the interactions with the neutral atoms and molecules, and the impact of the interactions on the plasma transport is subject to current attention in both experiments [2, 3] and simulations [4–12]. In particular, such effects as fuelling, divertor detachment [1, 13–15] and SOL density shoulder formation [2, 16–20], depend on the plasma-neutral interactions.

A successful approach to modeling the plasma edge and SOL dynamics is to describe the plasma in the two-fluid picture [21], where ions and electrons each constitute a fluid with its own density, momentum, and temperature, although the charge densities of electrons and ions are commonly assumed equal due to quasi-neutrality. The family of edge and SOL codes [4–7, 9–12], based on the two-fluid model, are extended within the past years to additionally model transport of neutral particles and the corresponding sources to the fluid plasma species.

Certain experimental observations in the edge and SOL regions, such as a deviation from a Gaussian ion velocity distribution to one with a lower temperature peak during shoulder formation [19] and measurements of co-existing neutral atoms at characteristic temperatures [22, 23] are, however, beyond the modeling capabilities of fluid models due to their restrictive assumption of a Maxwellian velocity distribution function for the continuum. Collisions generally drive the velocity distribution function towards that of a Maxwellian, whereas sources can contribute to a drive away from that. Regions with a high source rate compared to the collision rate pose an uncertainty in the applicability of fluid models.

The aforementioned observations are examples of kinetic effects that move the velocity distribution away from a Maxwellian function. While fluid-like descriptions of continua with non-Maxwellian distribution functions is an actively researched field [24, 25], a generic fluid description of a non-equilibrium continuum is lacking and may very well not exist, although some success was found in certain limit cases. For limit cases where the drive towards a single-Maxwellian velocity distribution function is sufficiently small, however, the distribution function may be described by a multi-Maxwellian distribution function, i.e., a sum of single-Maxwellian distribution functions, if the sources each follow a Maxwellian distribution function.

As for the neutral-augmented two-fluid models the interest in multi-ion-species fluid models, required for describing, e.g., fusion plasmas with a deuterium-tritium fuel mixture, is likewise increasing [9, 26]. The development of such models also enables plasma models where a single ion species is described by a multi-Maxwellian distribution function. In tandem with the source terms that arise from introducing neutral interactions, such a model may possibly describe the kinetic effects on the ion species arising from, e.g., the ionization of neutrals.

In this paper, we re-derive the self-consistent fluid source terms from kinetic operators and discuss how a fluid picture interprets the kinetic effects introduced by ionization. A multi-ion drift-fluid model (nMIHESEL), which in its essence combines transport and interactions with neutrals, nHESEL [5], with a multi-component plasma transport model, MIHESEL [26], is applied to model the neutral-populated SOL and edge regions, where the ionization source rate in the hot and dense plasma perturbations (blobs) may be high compared to the collision rate. The study considers blob scenarios using both a (conventional) single-Maxwellian and a double-Maxwellian velocity distribution fluid model. The results demonstrate that in the limit of a high source- to collision-rate ratio, which may be relevant for plasma filaments (blobs) in magnetically confined plasmas, the filamentary cross-field transport causes a different evolution of the density from that where a single-Maxwellian is assumed. The difference, however, is not to an extent that calls for a reevaluation of existing plasma fluid models of perpendicular transport with fluid interactions.

The paper is structured as follows. In Section 2 generic fluid source terms are re-derived from kinetic velocity space operators and the physical interpretation of the terms, in particular, an anomalous emergent heating term, is discussed. The underlying cause of the term is a failure of the fluid picture to describe the kinetic effects of a non-Maxwellian velocity distribution function. Section 3 sets out to investigate the impact of this kinetic effect by comparing simulations of seeded blobs described by either a single-Maxwellian or a double-Maxwellian drift-fluid model. The conclusions are summarized in Sec. 4.

2 Source terms in fluids and magnetized plasmas

The source terms that arise from the dominant inelastic interactions between charged particles and neutrals are well established and can be found in e.g. [5, 27, 28]. In the following section, Sec. 2.1, we do, however, sketch the derivation for these generic source terms to a fluid, originating from adding kinetic sources of amplification, advection, and diffusion in velocity space, to support the subsequent discussion. In Section 2.2 the form of the ionization sources, in terms of the generic sources, is provided. A particular term, that effectively heats the ions without the presence of an underlying physical mechanism to explain such heating, is moreover discussed in detail in Sec. 2.3.

2.1 Moments of kinetic source terms

The onset for the analysis of fluid source terms is the Boltzmann kinetic equation

$$\partial_t f_\sigma + \partial_{\boldsymbol{x}} \cdot (\boldsymbol{v} f_\sigma) + \partial_{\boldsymbol{v}} \cdot (\boldsymbol{a} f_\sigma) = \mathcal{C}_\sigma(f) + \mathcal{S}_\sigma(f)\,, \tag{1}$$

for the distribution function for particle species σ, $f_\sigma = f_\sigma(t; \boldsymbol{x}, \boldsymbol{v})$. On the right-hand side of (1) are the collision operator $\mathcal{C}_\sigma(f)$, where the absence of an index on the argument indicates that also other distribution functions than that for species σ are involved, and the source operator $\mathcal{S}_\sigma$.

The fluid equations are readily obtained in the Chapman-Enskog closure scheme by calculating the velocity-space moment equations for (1) while assuming that the distribution function $f_\sigma \equiv f_\sigma^{\mathrm{M}}$ is Maxwellian

$$f_\sigma^{\mathrm{M}}(t; \boldsymbol{x}, \boldsymbol{v}) = n_\sigma \left(\frac{m_\sigma}{2\pi T_\sigma}\right)^{\frac{3}{2}} \exp\left(-\frac{m_\sigma}{2T_\sigma}(\boldsymbol{v} - \boldsymbol{u}_\sigma)^2\right)\,, \tag{2}$$

where $n_\sigma = n_\sigma(t; \boldsymbol{x})$ is the particle density, $\boldsymbol{u}_\sigma = \boldsymbol{u}_\sigma(t; \boldsymbol{x})$ is the flow velocity, $T_\sigma = T_\sigma(t; \boldsymbol{x})$ is the temperature, and m_σ is the mass of particle species σ. The (contracted) moment integrated terms are identified as the fluid variables

$$n_\sigma(t; \boldsymbol{x}) \equiv \int \mathrm{d}^3 v\, f_\sigma(t; \boldsymbol{x}, \boldsymbol{v})\,, \tag{3}$$

$$\boldsymbol{\Gamma}_\sigma(t; \boldsymbol{x}) \equiv m \int \mathrm{d}^3 v\, \boldsymbol{v} f_\sigma(t; \boldsymbol{x}, \boldsymbol{v})\,, \tag{4}$$

$$\mathcal{E}_\sigma(t; \boldsymbol{x}) \equiv \tfrac{1}{2} m \int \mathrm{d}^3 v\, v^2 f_\sigma(t; \boldsymbol{x}, \boldsymbol{v})\,, \tag{5}$$

where $\boldsymbol{\Gamma}_\sigma = m_\sigma n_\sigma \boldsymbol{u}_\sigma$ is the momentum density and $\mathcal{E}_\sigma = \frac{1}{2} m_\sigma n_\sigma u_\sigma^2 + \frac{3}{2} n_\sigma T_\sigma$ is the energy density for the Maxwellian velocity distribution.

The collision operator is typically assumed to be bi-linear, but in the forthcoming analysis, the exact form of the collision terms is not crucial, although the associated characteristic collision frequency will play a role in defining the schemes in which the fluid approximation is valid.

Both the collision operator, which accounts for elastic collisions between particles in f_σ and those in the $f_{\sigma'}$ distribution functions, and the source operator, which accounts for all other interactions (including inelastic collisions), potentially involve other distribution functions and the index on the argument in (1) is thus omitted. The moments of the source operator are defined in agreement with (3-5)

$$S_\sigma^n(t; \boldsymbol{x}) \equiv \int \mathrm{d}^3 v\, \mathcal{S}_\sigma(t; \boldsymbol{x}, \boldsymbol{v})\,, \tag{6}$$

$$\boldsymbol{S}_\sigma^\Gamma(t; \boldsymbol{x}) \equiv m_\sigma \int \mathrm{d}^3 v\, \boldsymbol{v} \mathcal{S}_\sigma(t; \boldsymbol{x}, \boldsymbol{v})\,, \tag{7}$$

$$S_\sigma^\mathcal{E}(t; \boldsymbol{x}) \equiv \tfrac{1}{2} m_\sigma \int \mathrm{d}^3 v\, v^2 \mathcal{S}_\sigma(t; \boldsymbol{x}, \boldsymbol{v})\,. \tag{8}$$

We will consider two categories of kinetic source terms; those which correspond to a source only in one of the fluid variables n_σ, $\boldsymbol{u}_\sigma$, T_σ, i.e., by adding more particles at the same flow velocity and temperature as the existing fluid. The other category arises from the conversion of particles in $f_{\sigma'}$ to f_σ, such as ionization of neutrals, which potentially introduce a source to all fluid variables, since the created particles may have a different flow velocity and temperature than those of the bulk fluid.

The explicit form of kinetic source terms, which corresponds to only changing a single fluid parameter, denoted $\mathcal{S}_\sigma^\rho$ for $\rho = n_\sigma$, $\boldsymbol{u}_\sigma$, T_σ, can be found by writing the arguments of the Maxwellian distribution

function (2) in terms of the fluid variables, i.e., $f_\sigma^{\mathrm{M}}(t;\boldsymbol{x},\boldsymbol{v}) = f_\sigma^{\mathrm{M}}(\boldsymbol{v};n_\sigma(t;\boldsymbol{x}),\boldsymbol{u}_\sigma(t;\boldsymbol{x}),T_\sigma(t;\boldsymbol{x}))$ and calculate the change in f_σ^{M} due to changes in the individual fluid variables

$$\left[\frac{\mathrm{d}f_\sigma^{\mathrm{M}}(\boldsymbol{v};n_\sigma,\boldsymbol{u}_\sigma,T_\sigma)}{\mathrm{d}t}\right]_{\mathrm{S}} = \underbrace{\frac{\partial f_\sigma^{\mathrm{M}}}{\partial n_\sigma}\left[\frac{\mathrm{d}n_\sigma}{\mathrm{d}t}\right]_{\mathrm{S}}}_{\mathcal{S}_\sigma^n} + \underbrace{\frac{\partial f_\sigma^{\mathrm{M}}}{\partial \boldsymbol{u}_\sigma}\cdot\left[\frac{\mathrm{d}\boldsymbol{u}_\sigma}{\mathrm{d}t}\right]_{\mathrm{S}}}_{\mathcal{S}_\sigma^u} + \underbrace{\frac{\partial f_\sigma^{\mathrm{M}}}{\partial T_\sigma}\left[\frac{\mathrm{d}T_\sigma}{\mathrm{d}t}\right]_{\mathrm{S}}}_{\mathcal{S}_\sigma^T}\,. \tag{9}$$

For some field, $[\mathrm{d}_t\,\cdot]_{\mathrm{S}}$ represents the temporal change of that caused by a source. Denoting the corresponding fluid variable source terms

$$[\mathrm{d}_t n_\sigma]_{\mathrm{S}} \equiv \Sigma_\sigma^n(t;\boldsymbol{x})\,, \qquad [\mathrm{d}_t \boldsymbol{u}_\sigma]_{\mathrm{S}} \equiv \boldsymbol{\Sigma}_\sigma^u(t;\boldsymbol{x})\,, \qquad [\mathrm{d}_t T_\sigma]_{\mathrm{S}} \equiv \Sigma_\sigma^T(t;\boldsymbol{x})\,, \tag{10}$$

and using the known form of f_σ^{M} in (2) the source terms in (9) are readily evaluated

$$\mathcal{S}_\sigma^n(t;\boldsymbol{x},\boldsymbol{v}) = \frac{\Sigma_\sigma^n}{n_\sigma} f_\sigma^{\mathrm{M}}(t;\boldsymbol{x},\boldsymbol{v})\,, \tag{11}$$

$$\mathcal{S}_\sigma^u(t;\boldsymbol{x},\boldsymbol{v}) = \frac{m_\sigma}{T_\sigma}\left(\boldsymbol{v}-\boldsymbol{u}_\sigma\right)\cdot\boldsymbol{\Sigma}_\sigma^u\, f_\sigma^{\mathrm{M}}(t;\boldsymbol{x},\boldsymbol{v})\,, \tag{12}$$

$$\mathcal{S}_\sigma^T(t;\boldsymbol{x},\boldsymbol{v}) = \left(\frac{\frac{1}{2}m_\sigma\left(\boldsymbol{v}-\boldsymbol{u}_\sigma\right)^2}{T_\sigma} - \frac{3}{2}\right)\frac{\Sigma_\sigma^T}{T_\sigma} f_\sigma^{\mathrm{M}}(t;\boldsymbol{x},\boldsymbol{v})\,. \tag{13}$$

It is noted that the known form of the Maxwellian velocity distribution allows for obtaining the above explicit form for the kinetic source operators. For source operators acting on f_σ through respectively amplification, advection, and diffusion in velocity space, similar to the form of the Landau collision operator [29],

$$\mathcal{S}_\sigma^n\left(f_\sigma\right) \equiv A_\sigma f_\sigma(t;\boldsymbol{x},\boldsymbol{v})\,, \tag{14}$$

$$\mathcal{S}_\sigma^u\left(f_\sigma\right) \equiv \boldsymbol{B}_\sigma\cdot\partial_{\boldsymbol{v}} f_\sigma(t;\boldsymbol{x},\boldsymbol{v})\,, \tag{15}$$

$$\mathcal{S}_\sigma^T\left(f_\sigma\right) \equiv C_\sigma\partial_{\boldsymbol{v}}^2 f_\sigma(t;\boldsymbol{x},\boldsymbol{v})\,, \tag{16}$$

where the units of the coefficients are $[A_\sigma] = \mathrm{s}^{-1}$ (particle number source rate), $[B_\sigma] = \mathrm{m\,s}^{-2}$ (acceleration), and $[C_\sigma] = \mathrm{m}^2\mathrm{s}^{-3} = \mathrm{W\,kg}^{-1}$ (specific power) and for which it is straightforward to verify that the Maxwellian case have

$$A_\sigma = \frac{\Sigma_\sigma^n}{n_\sigma}\,, \qquad \boldsymbol{B}_\sigma = -\boldsymbol{\Sigma}_\sigma^u\,, \qquad C_\sigma = \frac{\Sigma_\sigma^T}{2m_\sigma}\,. \tag{17}$$

This form of the source operators (14-16) is also physically intuitive; a density source Σ_σ^n increases the amplitude of f_σ, a flow velocity source $\boldsymbol{\Sigma}_\sigma^u$ advects f_σ in velocity space, and a heating source Σ_σ^T results in a widening of f_σ in velocity space without changing the volume (density) or mean velocity (flow velocity). The physical mechanisms that would result in fluid source terms are, e.g., for Σ_σ^n addition of fluid at the same flow and temperature, for $\boldsymbol{\Sigma}_\sigma^u$ acceleration of the fluid by, e.g., applying an external electric field in the case of a charged fluid such as a plasma, and a finite Σ_σ^T could be obtained by heating the fluid without changing the density, e.g., by electromagnetic heating of the fluid particles. It is noted that for a plasma fluid, the flow velocity source from the acceleration due to an electric field is usually accounted for in the last term of the left-hand side of the Boltzmann equation (1) which has the same form as the flow velocity source term (15). The term is, however, preserved here for the sake of completeness. Also note that for a heat sink, due to, e.g., ionization for the electrons in a plasma, the kinetic heat source term results in anti-diffusion of the velocity distribution function.

What remains now is to calculate the moments of the kinetic source term, i.e., $\mathcal{S}_\sigma = \mathcal{S}_\sigma^n + \mathcal{S}_\sigma^u + \mathcal{S}_\sigma^T$, due to changes in the fluid variables, defined in (6-8). The fluid density source for a Maxwell distribution function is

$$S_\sigma^n(t;\boldsymbol{x}) = \int \mathrm{d}^3v\,\mathcal{S}_\sigma(t;\boldsymbol{x},\boldsymbol{v}) = \frac{\Sigma_\sigma^n}{n_\sigma}\int \mathrm{d}^3v\, f_\sigma^{\mathrm{M}}(t;\boldsymbol{x},\boldsymbol{v}) = \Sigma^n\,, \tag{18}$$

as only (14) has a finite integral value. The momentum density source is

$$\boldsymbol{S}_\sigma^\Gamma(t;\boldsymbol{x}) = m_\sigma\boldsymbol{u}_\sigma\Sigma_\sigma^n + m_\sigma n_\sigma\boldsymbol{\Sigma}_\sigma^u\,, \tag{19}$$

since only (14) and (15) have finite first moments. Similarly, the energy density source is

$$S_\sigma^{\mathcal{E}}(t;\boldsymbol{x}) = \left(\tfrac{1}{2}m_\sigma u_\sigma^2 + \tfrac{3}{2}T_\sigma\right)\Sigma_\sigma^n + m_\sigma n_\sigma\boldsymbol{u}_\sigma\cdot\boldsymbol{\Sigma}_\sigma^u + \tfrac{3}{2}n_\sigma\Sigma_\sigma^T\,. \tag{20}$$

The above expressions can be obtained equally from (11-13), (14-16) together with (17), or by applying the differentiation chain rule to the fluid expressions for $\mathbf{\Gamma}_\sigma$ and $\mathcal{E}_\sigma$ together with the definitions in (10).

In the following, we consider a plasma described as an electron fluid and an ion fluid and review the kinetic and fluid source terms that appear due to the ionization of a background fluid of neutral atoms of the same atomic number as the ions (e.g., a hydrogen plasma in a background of hydrogen atoms). Since the neutral fluid does not necessarily have the same flow velocity and temperature as the plasma fluids the task is more complicated than simply identifying an expression for Σ^n_σ and applying the previous framework.

2.2 Fluid variable source terms from ionization

The method of Sec. 2.1 is applicable if the velocity distribution of the particles added or removed by the density source Σ^n_σ has the same velocity space moments, i.e., flow velocity and temperature, as the bulk fluid described by f_σ. When a fluid, such as a plasma, is created, e.g., by ionization of neutral atoms, this is, however, not guaranteed. The sources must therefore be derived from (6-8) where, for ionization, the kinetic source term, $\mathcal{S}_\sigma$, depends on the neutral velocity distribution function f_n. A detailed derivation of the electron impact ionization fluid source terms can be found in, e.g., [28] and result in the source terms for density

$$\begin{aligned} S^n_{\mathrm{iz},\,\sigma} &= \int \mathrm{d}^3v'\, f_\mathrm{n}(\boldsymbol{v}') \int \mathrm{d}^3v\, f_\mathrm{e}(\boldsymbol{v})\sigma_\mathrm{iz} v_\mathrm{rel} \\ &\approx \int \mathrm{d}^3v' f_\mathrm{n}(\boldsymbol{v}') \int \mathrm{d}^3w\, f_\mathrm{e}(\boldsymbol{w})\sigma_\mathrm{iz}(w) w = n_\mathrm{n} n_\mathrm{e} \langle \sigma_\mathrm{iz} v_\mathrm{e}\rangle \equiv \Sigma^n_\mathrm{iz}\,, \end{aligned} \tag{21}$$

momentum density

$$\boldsymbol{S}^\Gamma_{\mathrm{iz},\,\sigma} = m_\sigma \int \mathrm{d}^3v'\, \boldsymbol{v}' f_\mathrm{n}(\boldsymbol{v}') \int \mathrm{d}^3v\, f_\mathrm{e}(\boldsymbol{v})\sigma_\mathrm{iz} v_\mathrm{rel} \approx m_\sigma \boldsymbol{u}_\mathrm{n} \Sigma^n_\mathrm{iz}\,, \tag{22}$$

and energy density

$$\begin{aligned} S^\mathcal{E}_{\mathrm{iz},\,\sigma} &= \tfrac{1}{2} m_\sigma \int \mathrm{d}^3v'\, v'^2 f_\mathrm{n}(\boldsymbol{v}') \int \mathrm{d}^3v\, f_\mathrm{e}(\boldsymbol{v})\sigma_\mathrm{iz} v_\mathrm{rel} \approx \left(\tfrac{1}{2} m_\sigma u_\mathrm{n}^2 + \tfrac{3}{2}\tfrac{m_\sigma}{m_\mathrm{n}} T_\mathrm{n}\right) \Sigma^n_\mathrm{iz} + \tfrac{3}{2} n_\sigma \Sigma^T_{\mathrm{iz},\,\sigma} \\ &= \left(\tfrac{1}{2} m_\sigma u_\mathrm{n}^2 + \tfrac{3}{2}\tfrac{m_\sigma}{m_\mathrm{n}} T_\mathrm{n} - \delta_{\sigma\mathrm{e}} \tfrac{3}{2}\phi_\mathrm{iz}\right) \Sigma^n_\mathrm{iz}\,, \end{aligned} \tag{23}$$

where the last equality is obtained by writing the heat sink for the electrons in terms of the electron ionization potential ϕ_iz. Note that the terms only describe sources from adding particles at distinct flow velocities and temperatures. Additional physical sources that may dominate in certain regimes, e.g., radiation at low temperatures, are not included.

The moments of the kinetic equation for an electron ($\sigma = \mathrm{e}$) or ion ($\sigma = \mathrm{i}$) species with an ionization source result in the Braginskii two-fluid equations [21] with auxiliary source terms

$$[\partial_t n_\sigma]_\mathrm{S} = S^n_{\mathrm{iz},\,\sigma}\,, \qquad [\partial_t \mathbf{\Gamma}_\sigma]_\mathrm{S} = \boldsymbol{S}^\Gamma_{\mathrm{iz},\,\sigma}\,, \qquad [\partial_t \mathcal{E}_\sigma]_\mathrm{S} = S^\mathcal{E}_{\mathrm{iz},\,\sigma}\,. \tag{24}$$

The interpretation of the sources is straightforward; all sources are proportional to the rate of particle creation, which also defines the density source in (21). The rate of gain in momentum density (22) by adding new particles is proportional to the rate at which the particles are created and to the momentum that the particles are created with, i.e., that defined by the flow velocity of the neutral fluid $\boldsymbol{u}_\mathrm{n}$. In particular, if the neutrals do not have a flow velocity there is no source from ionization to the momentum density of the plasma species. Similarly, the rate of growth of plasma species energy density (23) that results from adding new particles is proportional to the rate of particle creation. If the neutrals that are ionized have a finite flow velocity $\boldsymbol{u}_\mathrm{n}$ the first term in the brackets of (23) increases the energy density of the plasma species accordingly and similarly for the second term in case of neutrals with a finite temperature T_n. There is thus no gain in energy density if the neutrals are static and cold. The last term in (23), only present for electrons, is the sink in electron energy from the ionization process.

It is, however, more instructive to consider the set of ionization sources to the fluid variables used to parametrize the distribution function, i.e., $S^n_{\mathrm{iz},\,\sigma}$, $\boldsymbol{S}^u_{\mathrm{iz},\,\sigma}$, $S^T_{\mathrm{iz},\,\sigma}$. The latter two are defined by the right-hand sides of the equations

$$[\partial_t \boldsymbol{u}_\sigma]_\mathrm{S} = \boldsymbol{S}^u_{\mathrm{iz},\,\sigma}\,, \qquad [\partial_t T_\sigma]_\mathrm{S} = S^T_{\mathrm{iz},\,\sigma}\,, \tag{25}$$

and are obtained by subtracting lower moment equations from the momentum density and energy density equations respectively. The flow velocity source is thus

$$\begin{aligned}\partial_t \boldsymbol{u}_\sigma &= \frac{1}{n_\sigma}\left(\frac{1}{m_\sigma}\partial_t \boldsymbol{\Gamma}_\sigma - \boldsymbol{u}_\sigma \partial_t n_\sigma\right) = \frac{1}{n_\sigma}\left(\frac{1}{m_\sigma}\boldsymbol{S}^{\Gamma}_{\mathrm{iz},\,\sigma} - \boldsymbol{u}_\sigma S^n_{\mathrm{iz},\,\sigma}\right) \\ &= \left(\boldsymbol{u}_\mathrm{n} - \boldsymbol{u}_\sigma\right)\frac{\Sigma^n_\mathrm{iz}}{n_\sigma}\,.\end{aligned} \tag{26}$$

As opposed to the momentum density (22), ionization is a sink to the flow velocity if the ionized neutrals are static ($\boldsymbol{u}_\mathrm{n} = \boldsymbol{0}$), whereas the source term vanishes if the neutrals have the same flow velocity as the plasma species ($\boldsymbol{u}_\mathrm{n} = \boldsymbol{u}_\sigma$). On the path to obtaining the temperature source, one finds the pressure source

$$\begin{aligned}\partial_t p_\sigma &= \tfrac{2}{3}\left(\partial_t \mathcal{E}_\sigma - \tfrac{1}{2}m_\sigma \partial_t\left(n_\sigma u_\sigma^2\right)\right) \\ &= \tfrac{2}{3}\left(S^{\mathcal{E}}_{\mathrm{iz},\,\sigma} - \left(\tfrac{1}{2}m_\sigma u_\sigma^2 S^n_{\mathrm{iz},\,\sigma} + m_\sigma n_\sigma \boldsymbol{u}_\sigma \cdot \boldsymbol{S}^u_{\mathrm{iz},\,\sigma}\right)\right) \\ &= \left(\tfrac{1}{3}m_\sigma\left(\boldsymbol{u}_\mathrm{n} - \boldsymbol{u}_\sigma\right)^2 + \tfrac{m_\sigma}{m_\mathrm{n}}T_\mathrm{n} - \delta_{\sigma\mathrm{e}}\phi_\mathrm{iz}\right)\Sigma^n_\mathrm{iz}\,,\end{aligned} \tag{27}$$

which readily yields the temperature source

$$\begin{aligned}\partial_t T_\sigma &= \frac{1}{n_\sigma}\left(\partial_t p_\sigma - T_\sigma \partial_t n_\sigma\right) = \frac{1}{n_\sigma}\left(S^p_{\mathrm{iz},\,\sigma} - T_\sigma S^n_{\mathrm{iz},\,\sigma}\right) \\ &= \left(\tfrac{1}{3}m_\sigma\left(\boldsymbol{u}_\mathrm{n} - \boldsymbol{u}_\sigma\right)^2\right)\frac{\Sigma^n_\mathrm{iz}}{n_\sigma} + \left(\tfrac{m_\sigma}{m_\mathrm{n}}T_\mathrm{n} - T_\sigma\right)\frac{\Sigma^n_\mathrm{iz}}{n_\sigma} - \delta_{\sigma\mathrm{e}}\phi_\mathrm{iz}\frac{\Sigma^n_\mathrm{iz}}{n_\mathrm{e}}\,.\end{aligned} \tag{28}$$

The third term on the right-hand side of (28) is the temperature sink due to the ionization reaction, and the second term is, similar to that for the flow velocity in (26), a change in the temperature, depending on whether the thermal speed for the particles in the ionized fluid is smaller or larger than that for the resulting fluid. The nature of the first term on the right-hand side of (28) is, at first sight, perhaps somewhat less intuitive than the other source terms that have been reviewed. The term is positive definite unless $\boldsymbol{u}_\mathrm{n} = \boldsymbol{u}_\sigma$ in which case it vanishes. What makes this term peculiar is exactly the dependency on the neutral and charged particle flow velocities and that a difference in the two generates heat even in a plasma that is assumed to be collisionless. The physical interpretation of this term is discussed in Sec. 2.3.

To conclude the subsection, and for future reference, and before diving into a more deliberate discussion of the flow velocity dependent heat source term in Sec. 2.3 the flow velocity and temperature source terms are restated separately from their derivation in (26) and (28)

$$\boldsymbol{S}^u_{\mathrm{iz},\,\sigma} = \left(\boldsymbol{u}_\mathrm{n} - \boldsymbol{u}_\sigma\right)\frac{\Sigma^n_\mathrm{iz}}{n_\sigma}\,, \tag{29}$$

$$S^T_{\mathrm{iz},\,\sigma} = \left(\tfrac{1}{3}m_\sigma\left(\boldsymbol{u}_\mathrm{n} - \boldsymbol{u}_\sigma\right)^2\right)\frac{\Sigma^n_\mathrm{iz}}{n_\sigma} + \left(\tfrac{m_\sigma}{m_\mathrm{n}}T_\mathrm{n} - T_\sigma\right)\frac{\Sigma^n_\mathrm{iz}}{n_\sigma} - \delta_{\sigma\mathrm{e}}\phi_\mathrm{iz}\frac{\Sigma^n_\mathrm{iz}}{n_\mathrm{e}}\,. \tag{30}$$

It is noted that the form of the source terms provided here, despite being derived without consideration of magnetization of the plasma, are identical to those for a magnetized plasma. This correspondance is not obvious, as the ionized particles immidiately drift with their gyro-center velocities independent of their velocity before ionization. The derivation and interpretation are provided in App. A.

2.3 Does ionization heat the ions?

Consider the ions in a homogeneous one-dimensional collisionless plasma with fluid variables $n_0,\ u_0,\ T_0$ and thus with the velocity distributed according to the Maxwellian distribution function $f^\mathrm{M}_0 \equiv f^\mathrm{M}(v; n_0, u_0, T_0)$ for f^M given by (2). Now introduce a homogeneous density source by adding particles from another distribution function f^M_1 with fluid variables $n_1,\ u_1,\ T_1$. Note that we are now describing the system by two distribution functions. One could equally analyze this for the electron population, but the term of interest (i.e., the first term of (30)) is more relevant for the ion population due to their larger mass. The evolution of the fluid variables, and thus the velocity distribution function, is prescribed by the resulting source terms in (21, 29-30) by matching the indices to those above, i.e., $\sigma = 0$, n = 1. For the case of some $u_1,\ T_1 < u_0,\ T_0$ the evolution of the distribution function f is sketched in Fig. 1. For the case considered, adding new ions that are slower and colder to the system has the effect of increasing the density, slowing down the flow, and increasing the temperature. That the addition of ions results in a

heating of the system, even though the added ions are colder, is due to the difference in the flow velocities of the original ions and neutrals, which causes the flow velocity-dependent term in (30) to exceed that which depend on the temperature difference. The physical process, by which flow velocity is converted into heat, may not be obvious, but comes from the logical fallacy that the system is collisionless while maintaining a Maxwellian velocity distribution.

Note that the fluid equations for collisional fluids have terms of the exact same form as those in (29-30), with the source rate $\Sigma_{\mathrm{iz}}^n/n_\sigma$ replaced by the collision frequency [21]. In such case, the term corresponding to that in question is interpreted as frictional heating from collisions, which is required to drive the velocities towards a Maxwell-Boltzmann distribution.

Without collisions, there is no physical reason to treat the original and newly created ions as one fluid. If one desires to describe a truly collisionless system a more appropriate approach in the collisionless limit, or at least in the limit where the source rate is much larger than the rate of thermalization, may be treating the total velocity distribution as a double Maxwellian defined by the sum of two Maxwellian distribution functions; one for the original ions and one for the ions created in the ionization process

$$\begin{aligned} f(t;x,v) &= f_0^{\mathrm{M}}(t;x,v) + f_1^{\mathrm{M}}(t;x,v) \\ &= f^{\mathrm{M}}(v;n_0,u_0,T_0) + f^{\mathrm{M}}(v;n_1,u_1,T_1)\,. \end{aligned} \tag{31}$$

In Figure 1 the evolution of the distribution function f_{M} for the ions described as a single fluid and the double Maxwellian distribution function f defined in (31) are sketched. It is apparent that as the density of the secondary ion species grows the assumption of a common Maxwellian distribution function becomes increasingly incorrect. The interpretation of the source terms in (29-30) is now straightforward; there is no physical mechanism responsible for the change in flow velocity and temperature. The source terms simply describe how to evolve a single Maxwellian velocity distribution to fit a double Maxwellian velocity distribution function better under the conservation of momentum and energy. Ionization does not heat the ions if the system is treated properly.

Describing a collisionless system as a fluid may appear as an incorrect starting point in the first place. The reason for doing so is to highlight the origin of the source terms (29-30), which appear independent of collisionality and initiate the discussion of the (lack of) underlying physical mechanism.

In this section, the source terms for non-magnetized and magnetized plasmas have been laid out. It is highlighted how describing the fluid by a single Maxwellian velocity distribution function leads to a source term that interprets as a heating term when introducing particles with a different flow velocity, e.g., from ionization in a plasma. While this kinetic effect may be present in fusion plasmas, the magnitude of its impact on the plasma transport is not obvious. In Section 3 we investigate the implications of the effect on seeded blob cross-field transport when considering regimes of both small and large $\Sigma_{\mathrm{iz}}^n/n_\sigma$ to thermalization rate ratios. This is done while describing the ions either by a single or double Maxwellian velocity distribution function.

3 Numerical simulation of seeded filaments

In this section, we model and discuss the kinetic effects of ionized ions that have different flow velocities and temperatures compared to the main species. Section 3.1 describes the multi-species drift-fluid model equations and the implementation of the single-Maxwellian and double-Maxwellian distribution function (sMDF and dMDF) models. The simulation parameters are provided in Sec. 3.2 and the simulation results, i.e., the kinetic effects of the ionization process on seeded blob dynamics, are presented and discussed in Sec. 3.3.

3.1 nMIHESEL model equations

The neutral atoms are modeled as a static background fluid with density n_{n}, flow velocity $\boldsymbol{u}_{\mathrm{n}} = \mathbf{0}$, and (Franck-Condon) temperature $T_{\mathrm{n}} = 2\,\mathrm{eV}$. The temperature of the neutral atoms is that of a deuterium atom that originates from a dissociated deuterium molecule. While the nMIHESEL model allows for dynamic modeling of both interactions and transport of atoms and molecules, a static background of atoms, and no molecules, is applied here to focus the study. The ionization reaction rate Σ_{iz}^n is given by (21), and where the ionization reaction rate coefficient $\langle\sigma_{\mathrm{iz}}v\rangle$ is a function of the electron temperature and obtained from [30]. The neutral model is a limit case of that in nHESEL [5] with static neutrals and only ionization considered.

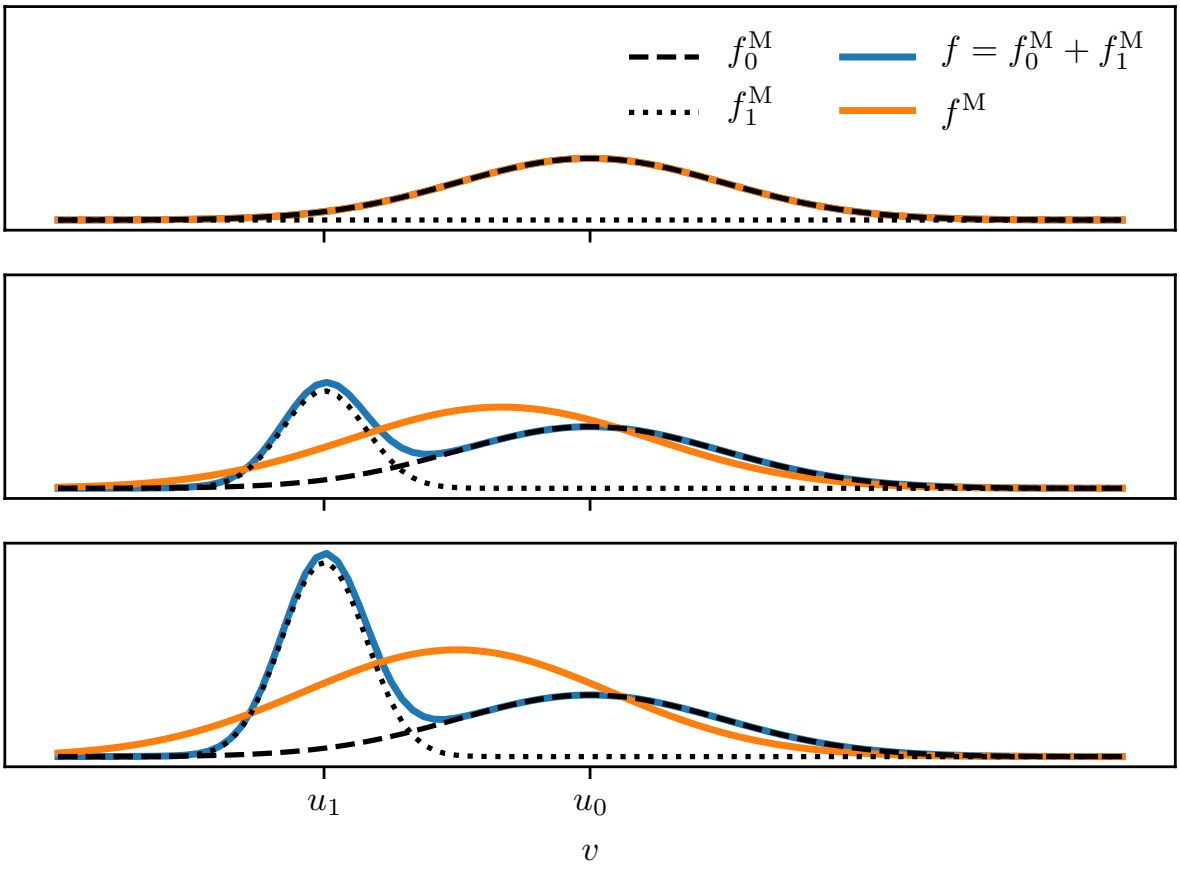

Figure 1: Sketch of the evolution (frame-wise from top and downwards) of the velocity distribution function for a collisionless fluid with a density source. The top plot shows the initial distributions and the plots below show the distributions at later times. f_0^{M} is the distribution function for the initial fluid and f_1^{M} is that for the newly created fluid at lower temperature and flow velocity. The distribution function denoted $f = f_0^{\mathrm{M}} + f_1^{\mathrm{M}}$ is the actual distribution function for the total fluid, whereas f^{M} is that which is obtained from evolving the Maxwellian f_0^{M} under conservation of momentum and energy. It is conventional to assume f^{M} as the velocity distribution function when modeling plasmas as fluids.

The evolution of the charged particle species is governed by the MIHESEL equations [26] augmented with the source terms from nHESEL described in Secs. 3.1.1 and 3.1.2. The full model, denoted nMIHESEL, describes the evolution of all individual ion species within a multi-ion species drift-fluid plasma. For ion species α the fluid is characterized by its ion densities n_α, ion pressures p_α, electron pressure p_e and $\mathbf{E}\times\mathbf{B}$-vorticity ω. The set of equations is closed according to the 21-moment Zhadanov closure [31] and can be found in B.

For the full set of MIHESEL equations and their origins, the reader is referred to B and [26] for the full derivation.

For this particular study two cases of the nMIHESEL equations are realized; one that treats the plasma as a conventional two-fluid with a single-ion component, and another that describe the plasma as a fluid with two ion components of the same species but with individual densities and pressures. The first case describes the ion velocity distribution function by a single-Maxwellian distribution function (sMDF), whereas the second case describes it by a double-Maxwellian distribution function (dMDF). The source terms for the two realizations are provided in Secs. 3.1.1 and 3.1.2 respectively. The electron species thermalize by a factor of the square root of the mass ratio faster than the ions and their velocity distribution function is described by a sMDF.

The aim of the simulations is to investigate if there is a significant difference between describing the ions by the conventional sMDF velocity distribution or the dMDF velocity distribution, which may be more proper to use in cases with subspecies of particles with another temperature. Two cases are investigated for each velocity distribution function; one where the collisionality rate is much larger than the source rate, $\nu_\mathrm{col} \gg \nu_\mathrm{iz}$, and one where the opposite is the case, $\nu_\mathrm{iz} \gg \nu_\mathrm{col}$. This totals the number of four simulation cases that are summarized in Table 1.

Table 1: The four study cases cover simulations with single and double Maxwellian distribution functions (sMDF and dMDF) in the collision and source-dominated regimes ($\nu_\mathrm{col} \gg \nu_\mathrm{iz}$ and $\nu_\mathrm{iz} \gg \nu_\mathrm{col}$)

	sMDF	dMDF
$\nu_\mathrm{col} \gg \nu_\mathrm{iz}$	Case 1	Case 2
$\nu_\mathrm{iz} \gg \nu_\mathrm{col}$	Case 3	Case 4

Intuitively one would expect Cases 1 and 2 to yield similar results since the collisions force the distribution functions towards their shared Maxwellian form faster than the new ions are created from ionization, whereas Cases 3 and 4 may differ for opposite reasons.

The temperature dependence of ν_col and ν_iz, as well as their temperature-dependent ratio, is shown in Fig. 2. To access the high collision-to-source rate regime, for cases 1 and 2, the seeded blob is given a lower temperature than that in cases 3 and 4, which is consequently initiated at a low collision-to-source rate. In the following, the source terms are explicitly given for the sMDF and dMDF cases. The full system of equations, including source terms, is also given in App. B.

3.1.1 Sources for the sMDF cases

The plasma is a single-species two-fluid with the additional source terms from the ionization of neutral atoms

$$[\partial_t n_\mathrm{i}]_\mathrm{S} = \Sigma^n \,, \tag{32}$$

$$[\partial_t p_\mathrm{i}]_\mathrm{S} = \left[\tfrac{1}{3} m_\mathrm{i} u_\mathrm{i}^2 + T_\mathrm{n}\right] \Sigma^n \,, \tag{33}$$

$$[\partial_t p_\mathrm{e}]_\mathrm{S} = \left[\tfrac{1}{3} m_\mathrm{e} u_\mathrm{e}^2 + \mu T_\mathrm{n} - \phi_\mathrm{iz}\right] \Sigma^n \,, \tag{34}$$

$$[\partial_t \omega]_\mathrm{S} = -\nabla \cdot \left[\frac{\Sigma^n}{n_\mathrm{i}\Omega_\mathrm{ci}} \left(\frac{\nabla_\perp \phi}{B} + \frac{\nabla_\perp p_\mathrm{i}}{q_\mathrm{i} n_\mathrm{i} B} \right) \right] \,, \tag{35}$$

where the plasma variables are the ion density n_i, ion pressure p_i, electron pressure p_e, $\mathbf{E}\times\mathbf{B}$-vorticity ω and electric potential ϕ. $\Sigma^n = n_\mathrm{n} n_\mathrm{e} \langle \sigma_\mathrm{iz} v \rangle$ is the density source, Ω_ci is the ion gyro frequency, $\boldsymbol{u}_\mathrm{e} = \boldsymbol{u}_\mathrm{i}$ are the leading order plasma velocity from $\mathbf{E}\times\mathbf{B}$ advection, μ is the electron to ion mass ratio, and $T_\mathrm{n} = 2\,\mathrm{eV}$ is the neutral atom temperature.

It is noted that the vorticity source (35) replaces the flow velocity source of Sec. 2.2 in the drift-fluid picture. The vorticity source, for the case of a neutral flow velocity identical to the drift-velocity, is reproduced in the gyro-fluid picture [32, 33]. The flow velocity source that appears when the neutral flow

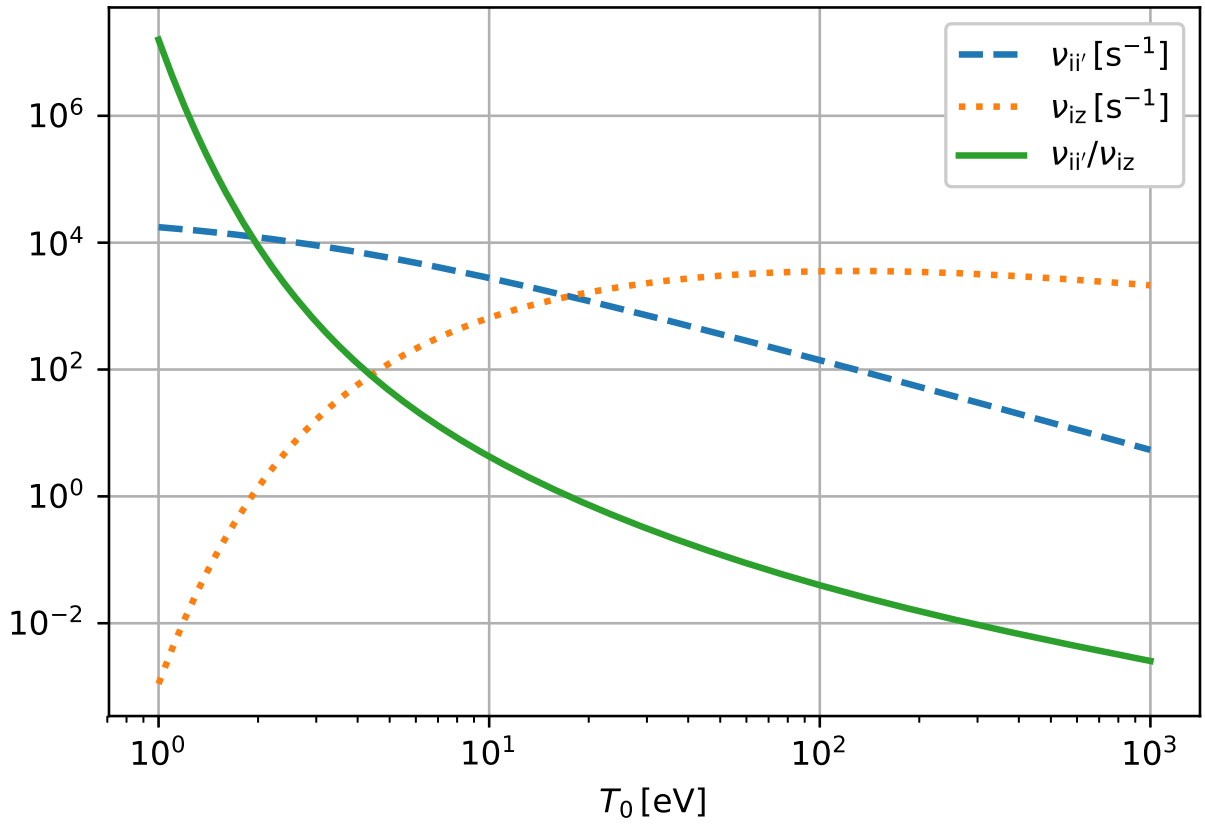

Figure 2: The temperature dependence of the ion-ion collisionality rate ν_{col}, the ionization rate ν_{iz} and the ratio between the two.

velocities are different from the drift-velocity, and which is described in App. A, is, however, not consistent with the gyro-fluid picture. This misalignment between the drift-fluid and gyro-fluid descriptions is a subject of future work.

3.1.2 Sources for the dMDF cases

The plasma is a double-species two-fluid with the additional source terms from the ionization of neutral atoms. One species is the original plasma (i.e., no sources) and the other species is that created by ionization.

$$[\partial_t n_1]_{\mathrm{S}} = 0\,, \tag{36}$$
$$[\partial_t p_1]_{\mathrm{S}} = 0\,, \tag{37}$$
$$[\partial_t n_2]_{\mathrm{S}} = \Sigma^n\,, \tag{38}$$
$$[\partial_t p_2]_{\mathrm{S}} = \left[\tfrac{1}{3} m_{\mathrm{i}} u_{\mathrm{i}}^2 + T_{\mathrm{n}}\right] \Sigma^n\,, \tag{39}$$
$$[\partial_t p_{\mathrm{e}}]_{\mathrm{S}} = \left[\tfrac{1}{3} m_{\mathrm{e}} u_{\mathrm{e}}^2 + \mu T_{\mathrm{n}} - \phi_{\mathrm{iz}}\right] \Sigma^n\,, \tag{40}$$
$$[\partial_t \omega]_{\mathrm{S}} = -\nabla \cdot \left[\frac{\Sigma^n}{n_2 \Omega_{\mathrm{ci}}} \left(\frac{\nabla_\perp \phi}{B} + \frac{\nabla_\perp p_2}{q_{\mathrm{i}} n_2 B}\right)\right]\,, \tag{41}$$

where the plasma variables are the ion densities $n_{1,2}$, ion pressures $p_{1,2}$, electron pressure p_{e}, $\mathbf{E}\times\mathbf{B}$-vorticity ω and electric potential ϕ.

3.2 Domain, parameters and initial conditions

The machine and plasma parameters are chosen to resemble those of a medium-sized tokamak with major radius $R = 1.5\,\mathrm{m}$, minor radius $a = 0.5\,\mathrm{m}$, on-axis magnetic field strength $B_0 = 2\,\mathrm{T}$, and safety factor at 95% of the minor radius $q_{95} = 5$, and a deuterium (mass number $A = 2$ and charge number $Z = 1$) plasma.

Table 2: Initial reference densities and temperatures for the four study cases.

		$\nu_{\mathrm{col}} \gg \nu_{\mathrm{iz}}$		$\nu_{\mathrm{iz}} \gg \nu_{\mathrm{col}}$	
		Case 1	Case 2	Case 3	Case 4
$n_{1,\mathrm{bkg}}$	$[\mathrm{m}^{-3}]$	10^{18}	10^{18}	10^{18}	10^{18}
$n_{2,\mathrm{bkg}}$	$[\mathrm{m}^{-3}]$	–	10^{15}	–	10^{15}
$T_{1,\mathrm{bkg}}$	[eV]	10	10	100	100
$T_{2,\mathrm{bkg}}$	[eV]	–	2	–	2

The initial conditions for the dMDF cases are provided below. For the sMDF cases, the conditions for $i = 1$ are applied. The primary density and temperature fields are initiated as Gaussian perturbations on a flat background and the secondary fields are homogeneous

$$f_i(t=0,x,y) = f_{i,\mathrm{bkg}} \left[1 + A_i \exp\left(-\frac{(x-x_0)^2 + (y-y_0)^2}{2\sigma^2}\right)\right] \tag{42}$$

with fields $f = n, T_{\mathrm{e,i}}$, background levels $f_{1,\mathrm{bkg}} = f_0$, $T_{2,\mathrm{bkg}} = T_{\mathrm{n}}$, $n_{2,\mathrm{bkg}} = 1 \cdot 10^{-3} n_0$ and perturbation amplitudes $A_1 = 1$, $A_2 = 0$. The density of the neutral background is $n_{\mathrm{n}} = 10^{16}\,\mathrm{m}^{-3}$. The physical values of the reference densities and temperatures are summarized in Table 2. The electrostatic potential is $\phi(0,x,y) = 0$ at initialization. The blob width is $\sigma = 10\rho_{\mathrm{s}}$, the domain is a square grid with physical side length $L = 40\sigma$, and the blob is initiated in the center at spatial position $x_0 = y_0 = L/2$. The equations are numerically solved using the Feltor discontinuous Galerkin library [34] on a grid resolved by $N_x = N_y = 360$ cells with three polynomial coefficients for a third-order method. Dirichlet boundary conditions are applied to all fields

$$\begin{aligned} f_i(t, x = \{0, L\}, y) = f_i(t, x, y = \{0, L\}) = f_{i,\mathrm{bkg}}\,, \\ \phi(t, x = \{0, L\}, y) = \phi(t, x, y = \{0, L\}) = 0\,. \end{aligned} \tag{43}$$

For this particular study the density source term in nMIHESEL is modified so only the perturbed electrons ionize neutrals, i.e., the density source is

$$\Sigma^n = (n_{\mathrm{e}} - n_{\mathrm{e,\,bkg}})\, n_{\mathrm{n}} \langle \sigma_{\mathrm{iz}} v \rangle\,. \tag{44}$$

The reason for this is, that the background pressure is mainly included for numerical reasons. If this is not subtracted from the source terms, a flat increase in plasma density occurs due to background ionization. The global increase in density does not provide new knowledge and moreover disturbs the effects of the ionization on the blob transport, and the cause of this is therefore subtracted.

3.3 Filament cross-field dynamics

In Figure 3 an instance of the blob density is shown at various time instances for all four simulation cases together with the absolute difference between cases 1 and 2, and cases 3 and 4. For all cases the blob develops asymmetrically due to a finite ion temperature and the warmer blob, with a higher ionization rate, is also observed to remain more coherent, which is consistent with the findings in [35–37]. The difference between the rightmost frames in Fig. 3a and Fig. 3d, which both show the density difference at time $t = 2.20\,\mu$s, is the largest among those displayed. The difference of applying a single MDF (cases 1 and 3) and a double MDF (cases 2 and 4) in the two scenarios at this point in time is almost three orders of magnitude.

Comparing the two scenarios at the same point in time may, however, not be the most appropriate basis for comparison. The ratio is qualitatively consistent with Sec. 2; a higher collisionality drives the two MDFs towards their common single MDF faster and the difference between those is therefore smaller. There are, however, other factors that may attribute to this difference that is not caused by the difference in collisionality-to-source ratio.

Part of the explanation for the larger difference could be attributed to the ionization rate being higher for the warmer cases with lower collisionality. To account for this the high collisionality cases are evolved to a point, τ_{iz}, where the ionization time is similar to that of the low collisionality cases at $t = 2.20\,\mu$s. The blob for cases 1 and 2 are shown at this time instance in Fig. 3b. Although the accounting for the difference in ionization time between the low and high collisionality reduces the discrepancies, the absolute differences in Figs. 3b and 3d still differ by almost two orders of magnitude.

Another explanation, that also relates to the different temperatures more than the difference in collisionality, is the difference in the blob evolution stages measured by their respective interchange times $\gamma^{-1} = \frac{\sqrt{R\sigma}}{2c_{\mathrm{s}}}$. Here R is the tokamak major radius, σ is the blob width according to (42) and $c_{\mathrm{s}} = \sqrt{\frac{T_{\mathrm{e}}}{m_{\mathrm{i}}}}$ is the ion acoustic speed [38]. Cases 1 and 2, with a temperature perturbation of 10 eV, have at $t = 2.20\,\mu$s evolved through $1.56\,\gamma^{-1}$, whereas the blob for cases 3 and 4 are shown at $4.94\,\gamma^{-1}$ according to their respective interchange time. Evolving cases 1 and 2 to the same point relative to the interchange time, τ_γ, as cases 3 and 4 in Fig. 3d, results in the density distributions for the high collisionality cases shown in Fig. 3c. At this stage, the low collisionality cases have evolved through a larger ionization time, but there persists to be an order of magnitude difference between the discrepancies between the single and double MDF cases for Figs. 3c and 3d.

In summary; Fig. 3 shows that the difference in describing a blob, that is subject to a density source from ionization, by either a single or double MDF is more pronounced at low collisionality compared to a similar system at higher collisionality. The difference is partly caused by the difference in ionization time and interchange time, but cannot solely be explained by those effects, and is therefore attributed to kinetic effects.

The influence of the kinetic effect on the blob motion is, however, not pronounced in the cross-field filament dynamics. A hypothesized reason for this draws on the conclusions from [36]; that the main contributor in altering filamentary cross-field dynamics is the $\mathbf{F}\times\mathbf{B}$-vorticity source. Inspecting the source terms (35) and (41) it appears that the source enters through gradient fields. Since the density source is proportional to the bulk plasma density, the spatial density distribution of the pressure of the plasma created from ionization is also similar to this, and the difference in the gradient terms in the vorticity sources is marginal. Thus, kinetic effects from ionization are believed to only weakly alter the dynamics due to their small divergence from the fluid vorticity source.

The kinetic effect is also visible in Fig. 4, where the ion temperatures for all four cases are shown. It is observed that for case 2 the temperature, T_2, of the ions that originate from ionization is almost 4 eV at its peak. The temperature of the ions from ionization in case 4, on the other hand, remains close to 2 eV, which is the temperature at which the ions in all cases are created. The Figure demonstrates that for a low-temperature filament, where the collisionality is high and the source rate low, a single Maxwellian is appropriate for describing the velocity distribution function of the ions. For higher temperatures, however, the collisionality is lower and the source rate is higher. In those cases, the temperature of the ions from ionization remains close to that at which they are created as the thermalization is slower than the rate of creation of new ions. A double Maxwellian may describe the velocity distribution function

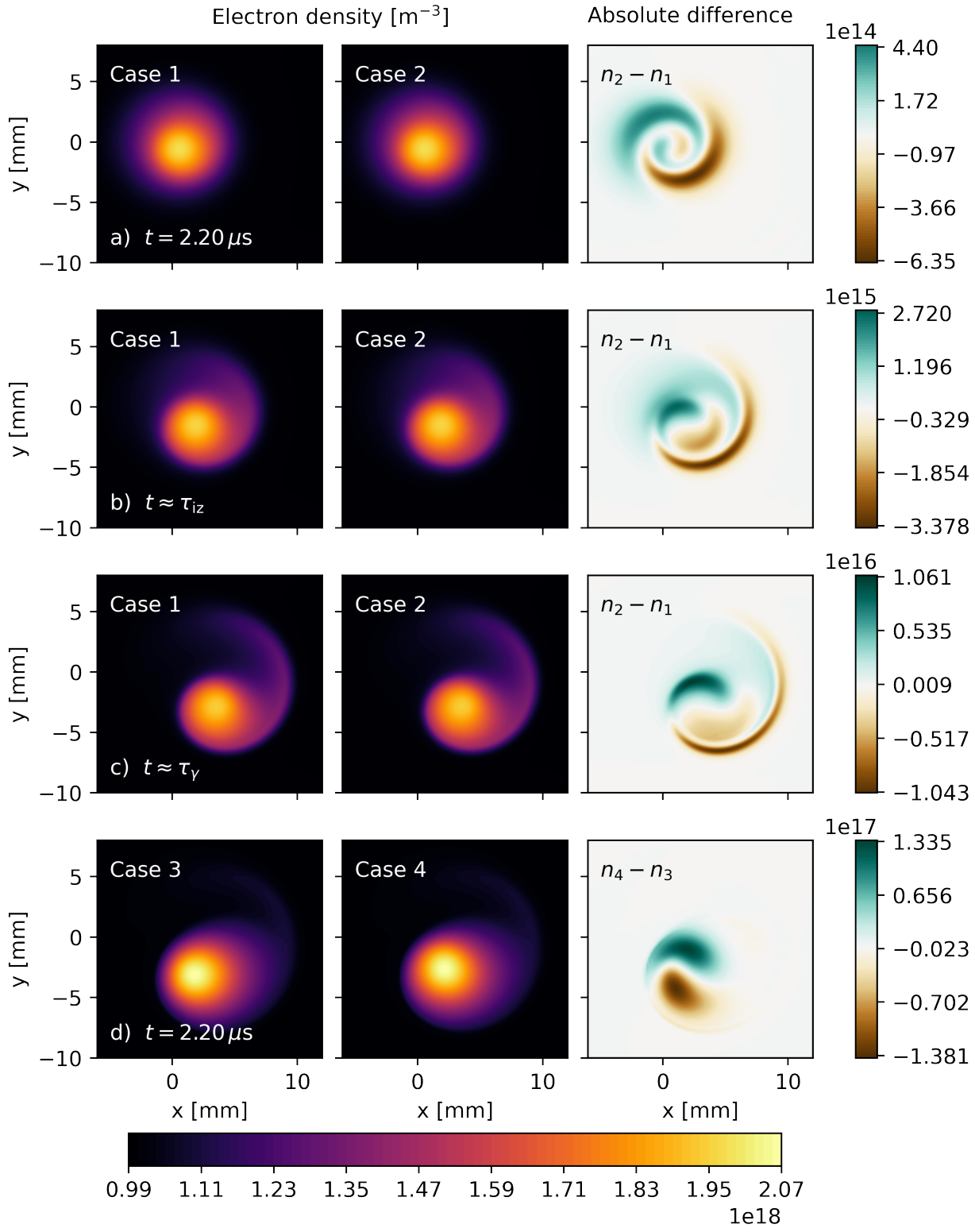

Figure 3: Evolution of seeded blob densities in the four cases. The first and last rows display the densities for all cases at time $t = 2.20\,\mu$s. The second and third rows show the density of the high collisionality cases after the same ionization and interchange times as that of the low collisionality cases. The rightmost frame of all rows shows the absolute difference between the densities in that row.

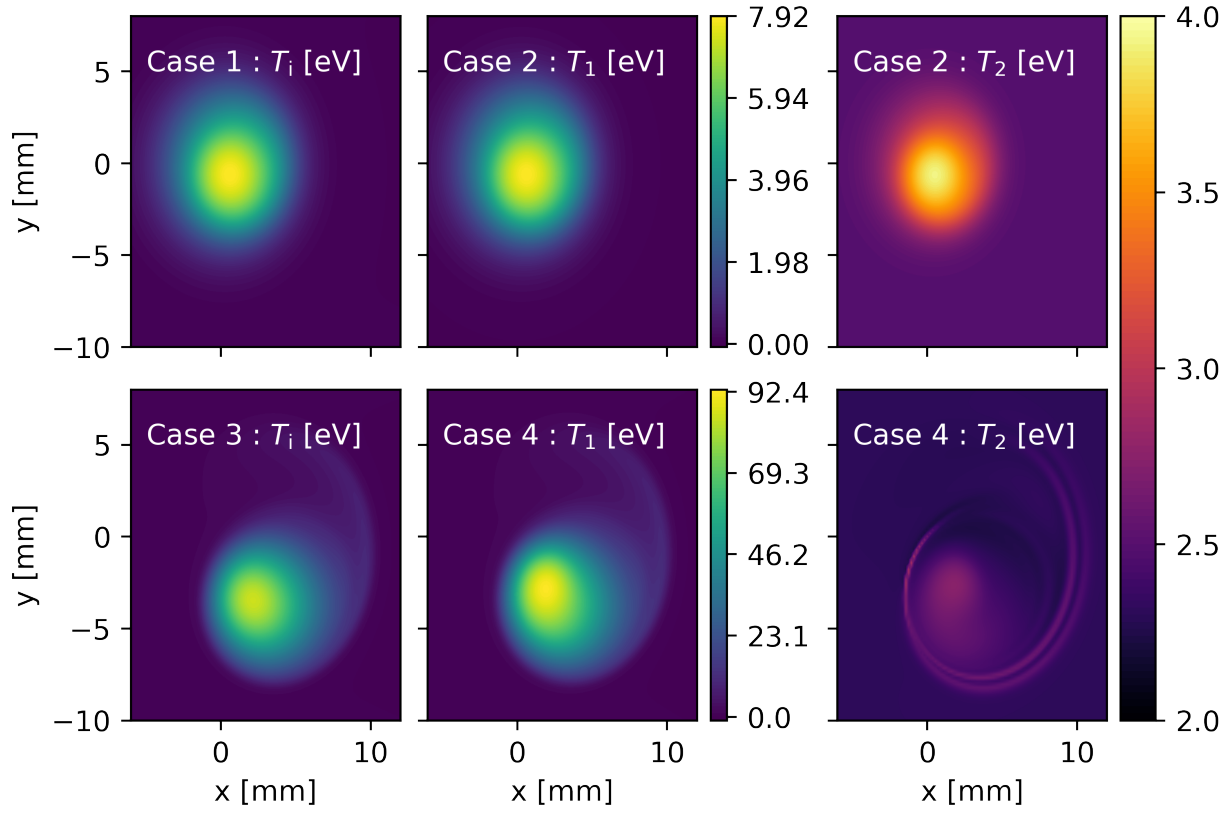

Figure 4: Evolution of seeded blob temperature perturbations in the four cases at time $t = 2.20\,\mu$s. For the dMDF cases, 2 and 4 both the main ion temperature and that of the ions that originate from ionization are shown. For case 2, the low-temperature case, the ions from ionization thermalize much faster than for the high-temperature case 4.

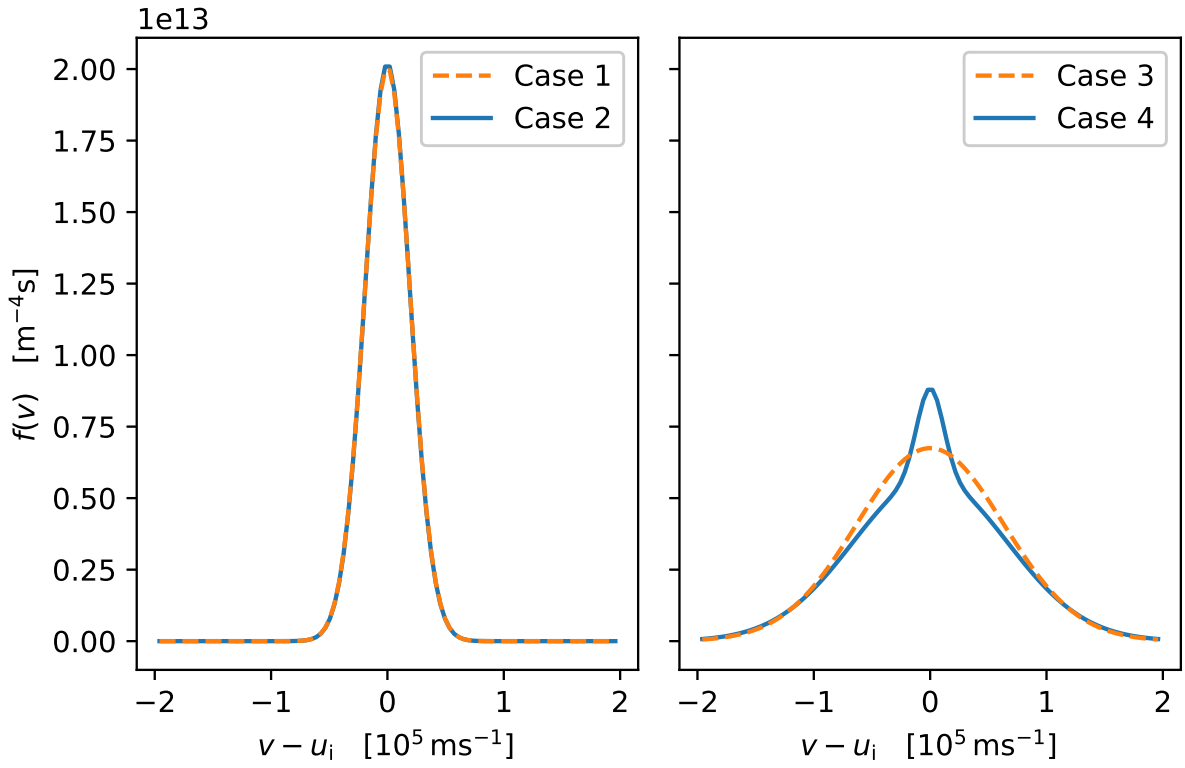

Figure 5: Velocity distribution functions corresponding to the fluid parameters at the peak density positions for the four blob cases shown in Figs. 3a and 3d.

better in those cases.

The kinetic effect is also visible from Fig. 5 in which the result of inserting the thermodynamic variables at the density peak positions in the MDFs prescribed by (2) for all four cases is shown. The figure illustrates clearly that the kinetic effect, while only weakly influencing the blob motion, is much more pronounced for the low collisionality double MDF case. The reason for this cannot only be attributed to the higher collisionality for cases 1 and 2, which drives the velocity distribution functions faster towards a shared form. The relative temperature difference between the bulk and ionized plasma species is much smaller for cases 1 and 2, compared to the low collisionality cases. Any perturbation to case 2 is therefore much less pronounced than for case 4.

We wish to highlight another interesting feature of magnetized plasmas, at least those where the drift-approximation is valid. Maxwellian velocity distribution function perturbations due to, e.g. ionization, will always align with the velocity distribution function of the bulk plasma around a shared flow velocity, as the ionized particles instantaneously move with the drift velocity. This results in Maxwellian perturbations, or any other perturbation with a peaked center at the mean velocity, which will have the largest perturbation amplitude where the background Maxwellian velocity distribution function is largest and thus minimizing the relative amplitude of the perturbation. This makes magnetized plasmas robust to this kind of perturbation as the error to the fluid approximation, i.e., kinetic effects, are likewise minimized. The larger variability of the velocity distribution in the direction parallel to the magnetic field lines is also known from gyrokinetic theory.

4 Conclusions

In certain magnetically confined plasma regions, such as the potentially neutral-rich SOL, and operation scenarios, such as NBI or pellet fuelling, the ionization source rate may be comparable to or larger than the rate of collisional thermalization. In those cases, the velocity distribution function of the bulk ion species may not be well described by a Maxwell-Boltzmann velocity distribution, which is commonly assumed in the fluid picture.

The potential kinetic effect on the transport of filamentary structures in a magnetized SOL plasma is investigated through the multi-species drift-fluid model nMIHESEL [5, 26] that allows for treating the bulk plasma and that created from ionization as separate fluids with individual temperatures. Seeded filaments are created in regimes of both high and low collision-to-source rates. In the high collision-to-source rate regime the drive towards a shared Maxwellian velocity distribution function is strong and the single and double Maxwellian distribution functions are shown to coincide. In the low collision-to-source rate the velocity distribution functions remain distinct but yet result in little difference in the evolution of the filament compared to that described by a single Maxwellian distribution function.

Several factors may contribute to the robustness of the filament dynamics to kinetic effects from ionization; due to the instantaneous acceleration of the flow velocity of ionized particles to the common drift velocity the perturbation on the bulk plasma velocity distribution function will always appear at its peak where the relative amplitude difference is the smallest. Temperature sources are likewise known to only affect the filamentary transport marginally [36], and due to the form of the self-consistent ionization source, the difference in the vorticity source between the sMDF and dMDF cases, which may have the largest potential for changing the dynamics, is vanishing.

In addition to the simulation analysis, it is illustrated how kinetic sources to particles with a Maxwellian velocity distribution function, which can be described as amplification, advection, or diffusion of the velocity distribution function, correspond to sources in the fluid variables density, flow velocity, and temperature respectively. The fluid source terms, assuming a Maxwellian velocity distribution function, have the characteristics of frictious heating, but with the ionization rate in place of the collision rate.

The study concludes that kinetic effects from ionization may be (continued) neglected in most current cross-field transport simulation scenarios of magnetized plasmas. The kinetic effects on transport parallel to the magnetic field lines, where the velocity distribution function does not exhibit the same robustness to perturbations may, however, influence the transport significantly and the topic is subject for future research.

This work has been carried out within the framework of the EUROfusion Consortium, funded by the European Union via the Euratom Research and Training Programme (Grant Agreement No 101052200

— EUROfusion). Views and opinions expressed are however those of the author(s) only and do not necessarily reflect those of the European Union or the European Commission. Neither the European Union nor the European Commission can be held responsible for them.

A Ionization source terms in magnetized plasmas

This appendix aims to aid the discussion on the form of the fluid ionization source terms. While, as it appears, the source terms provided in Sec. 2.2 are applicable also to a magnetized plasma, this is not obvious. The fluid source terms for the ionization process in Sec. 2.2 reflect the conservation of fluid momentum and energy in the ionization process. In magnetized plasmas, however, a neutral particle that is ionized becomes an ion that gyrates with its full perpendicular velocity. In the fluid picture, this corresponds to a conversion of some of its flow velocity to heat. The particle gyro-motion will, however, typically result in a drift-velocity, which constitutes the perpendicular momentum for the magnetized plasma fluid, independent of the flow velocity it had as a neutral. Only in the case where there is a homogeneous magnetic field and no other forces acting on the particle, the full flow velocity is converted to heat.

The leading order drift, the $\mathbf{E}\times\mathbf{B}$-drift, typically results from an external magnetic field and a self-organized internal electric field with components perpendicular to the magnetic field. Upon ionization, the position of the gyro-center relative to the position of the particle may be located further up or down the electrostatic potential depending on its perpendicular velocity. The rate of change in energy density is given by $m_\sigma \left(\boldsymbol{u}_{\sigma\perp}^2 - \boldsymbol{u}_{\mathrm{n}\perp}\cdot\boldsymbol{u}_{\sigma\perp}\right)\Sigma_{\mathrm{iz}}^n$ from work done by the electric field (or any other conservative force). The total energy density source for a magnetized plasma (indicated by $\star$) is

$$\begin{aligned}\left[S_{\mathrm{iz},\,\sigma}^{\mathcal{E}}\right]_\star &= \left(\tfrac{1}{2}m_\sigma u_{\mathrm{n}}^2 + m_\sigma\left(\boldsymbol{u}_{\sigma\perp}^2 - \boldsymbol{u}_{\mathrm{n}\perp}\cdot\boldsymbol{u}_{\sigma\perp}\right) - m_\sigma\boldsymbol{u}_{\sigma\perp}\cdot\left(\boldsymbol{u}_{\sigma\perp}-\boldsymbol{u}_{\mathrm{n}\perp}\right) + \tfrac{3}{2}\tfrac{m_\sigma}{m_{\mathrm{n}}}T_{\mathrm{n}} - \delta_{\sigma\mathrm{e}}\tfrac{3}{2}\phi_{\mathrm{iz}}\right)\Sigma_{\mathrm{iz}}^n\,,\\ &= \left(\tfrac{1}{2}m_\sigma u_{\mathrm{n}}^2 + \tfrac{3}{2}\tfrac{m_\sigma}{m_{\mathrm{n}}}T_{\mathrm{n}} - \delta_{\sigma\mathrm{e}}\tfrac{3}{2}\phi_{\mathrm{iz}}\right)\Sigma_{\mathrm{iz}}^n\,.\end{aligned} \tag{A.1}$$

Note how the work done has been accounted for in the first line by adding and subtracting the same term. The reason for writing this explicitly is that it gives a hint on the origin of the sink term in the energy density, $-m_\sigma\boldsymbol{u}_{\sigma\perp}\cdot\left(\boldsymbol{u}_{\sigma\perp}-\boldsymbol{u}_{\mathrm{n}\perp}\right)\Sigma_{\mathrm{iz}}^n$. Comparing the first line of (A.1) to the form of (20) one notices that the energy density sink term has the form of a flow velocity source contribution to the energy density, $m_\sigma n_\sigma \boldsymbol{u}_\sigma\cdot\boldsymbol{\Sigma}_\sigma^u$. The corresponding flow velocity source is $\boldsymbol{\Sigma}_\sigma^u = \left(\boldsymbol{u}_{\mathrm{n}\perp}-\boldsymbol{u}_{\sigma\perp}\right)\frac{\Sigma_{\mathrm{iz}}^n}{n_{\mathrm{e}}}$.

The fluid momentum density source term thus has an additional contribution to the flow velocity source deduced above. Following (19) the fluid momentum density source is

$$\begin{aligned}\left[\boldsymbol{S}_{\mathrm{iz},\,\sigma}^{\Gamma}\right]_\star &= m_\sigma\left(\boldsymbol{u}_\sigma\Sigma_{\mathrm{iz}}^n + n_\sigma\boldsymbol{\Sigma}_\sigma^u\right) = m_\sigma\left(\boldsymbol{u}_\sigma\Sigma_{\mathrm{iz}}^n + \left(\boldsymbol{u}_{\mathrm{n}}-\boldsymbol{u}_\sigma\right)\Sigma_{\mathrm{iz}}^n\right)\\ &= m_\sigma\boldsymbol{u}_{\mathrm{n}}\Sigma_{\mathrm{iz}}^n\,.\end{aligned} \tag{A.2}$$

The corresponding sources to flow velocity and temperature are

$$\left[\boldsymbol{S}_{\mathrm{iz},\,\sigma}^{u}\right]_\star = \left(\boldsymbol{u}_{\mathrm{n}}-\boldsymbol{u}_\sigma\right)\frac{\Sigma_{\mathrm{iz}}^n}{n_\sigma}\,, \tag{A.3}$$

$$\left[S_{\mathrm{iz},\,\sigma}^{T}\right]_\star = \tfrac{1}{3}m_\sigma\left(\boldsymbol{u}_{\mathrm{n}}-\boldsymbol{u}_\sigma\right)^2\frac{\Sigma_{\mathrm{iz}}^n}{n_\sigma} + \left(\tfrac{m_\sigma}{m_{\mathrm{n}}}T_{\mathrm{n}} - T_\sigma\right)\frac{\Sigma_{\mathrm{iz}}^n}{n_\sigma} - \delta_{\sigma\mathrm{e}}\phi_{\mathrm{iz}}\frac{\Sigma_{\mathrm{iz}}^n}{n_{\mathrm{e}}}\,. \tag{A.4}$$

The physical interpretation of the flow momentum source is, that the energy required to do the work on the ionized particles must come from the self-organized internal field that causes the drift. By doing work the energy of the field is changed. This again changes the local drift velocity, which reflects in the flow momentum source.

The source terms, (A.3) and (A.4), appear identical to those for the unmagnetized plasma (29) and (30). It is worth noting, however, that while the physics of the flow velocity term in the temperature source discussed in Sec. 2.3 are not obvious for the unmagnetized case, the term is much more easily explained in the magnetized case. In the magnetized case the perpendicular flow velocity of the ionized fluid is randomized into thermal gyro-motion except for the part of the flow velocity that aligns with the drift velocity. The term in the magnetized case thus represents an actual conversion of flow velocity to heat.

The actual drift velocity may originate from multiple forces of various origins. In the drift-fluid picture, however, it is typically assumed that the drift-velocity to leading order is provided by the $\mathbf{E}\times\mathbf{B}$-drift.

B nMIHESEL equations

The nMIHESEL equations are a set of equations that solve for the density and pressure evolution of the individual ion species and electrons under the quasi neutrality assumption $\sum_\alpha Z_\alpha n_\alpha = n_e$. The gyro-Bohm normalized equations are

$$\frac{d}{dt}n_\alpha + n_\alpha \mathcal{C}(\phi) + \frac{1}{Z_\alpha}\mathcal{C}(p_\alpha) - a_\alpha \frac{\mu_\alpha}{Z_\alpha}\nabla\cdot\left(\frac{d^0}{dt}\nabla_\perp \phi^*_\alpha\right) = \Lambda^n_\alpha + S^n_\alpha\,, \tag{B.1}$$

$$\sum_\alpha a_\alpha \mu_\alpha \nabla\cdot\left(\frac{d^0}{dt}\nabla_\perp \phi^*_\alpha\right) - \mathcal{C}\left(\sum_\alpha p_\alpha + p_e\right) = \Lambda^\omega + S^\omega\,, \tag{B.2}$$

$$\frac{3}{2}\frac{d}{dt}p_\alpha + \frac{5}{2}p_\alpha \mathcal{C}(\phi) + \frac{5}{2}\frac{1}{Z_\alpha}\mathcal{C}\left(\frac{p_\alpha^2}{n_\alpha}\right) - p_\alpha\frac{\mu_\alpha}{Z_\alpha}\nabla\cdot\left(\frac{d^0}{dt}\nabla_\perp\phi^*_\alpha\right) = \Lambda^p_\alpha + S^p_\alpha\,, \tag{B.3}$$

$$\frac{3}{2}\frac{d}{dt}p_\mathrm{e} + \frac{5}{2}p_\mathrm{e}\mathcal{C}(\phi) - \frac{5}{2}\mathcal{C}\left(\frac{p_e^2}{n_\mathrm{e}}\right) = \Lambda^p_\mathrm{e} + S^p_\mathrm{e}\,, \tag{B.4}$$

with generalized potential $\phi^*_\alpha = \phi + p_\alpha/Z_\alpha a_\alpha$. The right-hand side contains all interactions and source terms. The interaction terms are

$$\Lambda^n_\alpha = \sum_s \frac{D_{s\to\alpha,0}}{a_s\tau_\alpha}\nabla\cdot\left(T_\alpha n_s\nabla n_\alpha - \frac{Z_\alpha}{Z_s}T_s n_\alpha\nabla n_s\right) - \sum_\beta \frac{a_\alpha D_{\pi,\beta\to\alpha,0}}{\Omega_{c,\alpha,0}}\nabla^2\nabla^2\phi^*_\alpha\,, \tag{B.5}$$

$$\Lambda^\omega = \sum_\alpha\sum_\beta Z_\alpha \frac{a_\alpha D_{\pi,\beta\to\alpha,0}}{\Omega_{c,0,\alpha}}\nabla^2\nabla^2\phi^*_\alpha + \Xi_{\omega,\parallel}\,, \tag{B.6}$$

$$\begin{aligned}
\Lambda^p_\alpha =& \frac{5}{2}\sum_s \frac{D_{s\to\alpha,0}}{a_s}\nabla\cdot\left(T_\alpha n_s\nabla n_\alpha - \frac{Z_\alpha}{Z_s}T_s n_\alpha\nabla n_s\right) - p_\alpha\sum_\beta\frac{D_{\pi,\beta\to\alpha,0}}{\Omega_{c,\alpha,0}}\nabla^2\nabla^2\phi^*_\alpha \\
&- \sum_\beta \frac{D_{\beta\to\alpha,0}}{\mu_\alpha a_\beta}\mu_{\alpha\beta}\nabla\cdot\left(\frac{3}{2}\left[n_\beta\nabla p_\alpha - \frac{Z_\alpha}{Z_\beta}n_\alpha\nabla p_\beta\right]\right. \\
&\left. - \frac{\mu_\alpha}{\mu_\alpha+\mu_\beta}n_\alpha n_\beta\left[\left(\frac{13}{4}\frac{\mu_\beta}{\mu_\alpha} + 4 + \frac{15}{2}\frac{\mu_\alpha}{\mu_\beta}\right)\nabla T_\alpha - \frac{Z_\alpha}{Z_\beta}\frac{27}{4}\nabla T_\beta\right]\right) \\
&+ \sum_s \frac{D_{s\to\alpha,0}}{a_s\tau_\alpha}\left(T_\alpha n_s\nabla n_\alpha - \frac{q_\alpha}{q_s}T_s n_\alpha\nabla n_s\right)\cdot(q_\alpha\nabla\phi) \\
&+ \sum_\beta \mu_\alpha a_\alpha D_{\pi,\beta\to\alpha,0}\left[\left(\partial_x^2\phi^*_\alpha - \partial_y^2\phi^*_\alpha\right)^2 + 4\left(\partial_{xy}\phi^*_\alpha\right)^2\right] \\
&+ \sum_s \frac{3n_\alpha n_s\nu_{s\to\alpha,0}\mu_\alpha\left(T_s - T_\alpha\right)}{a_s(\mu_\alpha+\mu_s)} + \Xi_{p_\alpha,\parallel}\,,
\end{aligned} \tag{B.7}$$

$$\begin{aligned}
\Lambda^p_\mathrm{e} =& \sum_s \frac{D_{s\to\alpha,0}}{a_s\tau_\mathrm{e}}\nabla\cdot\left(T_e n_s\nabla n_\mathrm{e} - \frac{Z_\mathrm{e}}{Z_s}T_s n_\mathrm{e}\nabla n_s\right) + \sum_\alpha\left(1+\frac{\sqrt{2}}{Z_\alpha}\right)D_{\alpha\to\mathrm{e},0}\nabla\cdot(n_\mathrm{e}\nabla T_\mathrm{e}) \\
&+ \sum_s \frac{D_{s\to\mathrm{e},0}}{a_s}\left(T_\mathrm{e} n_s\nabla n_\mathrm{e} - \frac{q_\mathrm{e}}{q_s}T_s n_\mathrm{e}\nabla n_s\right)\cdot(q_\mathrm{e}\nabla\phi) + \sum_s\frac{3n_\mathrm{e}n_s\nu_{s\to e,0}\mu_\mathrm{e}\left(T_s - T_\mathrm{e}\right)}{a_s(\mu_\mathrm{e}+\mu_s)} + \Xi_{pe,\parallel}\,,
\end{aligned} \tag{B.8}$$

with constant parameters

$$m_s/m_\mathrm{Ref}\to\mu_s,\ n_{s,0}/n_{\mathrm{e},0}\to a_s,\ T_{s,0}/T_{\mathrm{e},0}\to\tau_s\,. \tag{B.9}$$

The total derivatives are defined as

$$\frac{d}{dt} = \frac{\partial}{\partial t} + \frac{1}{B}\{\phi,\cdot\} \quad \text{and} \quad \frac{d^0}{dt} = \frac{\partial}{\partial t} + \{\phi,\cdot\}\,. \tag{B.10}$$

with the Poisson brackets

$$\{f,g\} \equiv \partial_x f\partial_y g - \partial_y f\partial_x g\,. \tag{B.11}$$

The collision frequencies and diffusion coefficients are given by:

$$\nu_{s'\to s} = \frac{2^{1/2}n_{s'}Z_s^2Z_{s'}^2e^4\ln\Lambda_{ss'}\left(1+\frac{m_s}{m_{s'}}\right)}{12\pi^{3/2}\epsilon_0^2m_s^2\left(\frac{T_s}{m_s}+\frac{T_{s'}}{m_{s'}}\right)^{3/2}}\,. \tag{B.12}$$

where $\ln \Lambda_{ss'}$ is the coulomb logarithm for multiple ion species. From the collision frequency the diffusion coefficients are given:

$$D_{s'\to s} = \rho_s^2 \nu_{s'\to s} = \frac{\nu_{s'\to s} v_{\mathrm{th},s}^2}{\Omega_{\mathrm{c},s}^2}\,, \tag{B.13}$$

$$D_{\pi,\beta\to\alpha,0} = D_{\beta\to\alpha,0} \frac{m_\alpha m_\beta}{(m_\alpha + m_\beta)^2} \left(\frac{3}{10}\frac{m_\beta}{m_\alpha} + \frac{1}{2} - \frac{1}{5}\frac{m_\beta}{m_\alpha}\frac{Z_\alpha}{Z_\beta} \right). \tag{B.14}$$

References

[1] Peter C Stangeby. "Plasma Physics Series The Plasma Boundary of Magnetic Fusion Devices". In: (2000).

[2] N. Vianello, D. Carralero, C. K. Tsui, V. Naulin, M. Agostini, I. Cziegler, B. Labit, C. Theiler, E. Wolfrum, D. Aguiam, et al. "Scrape-off layer transport and filament characteristics in high-density tokamak regimes". In: *Nuclear Fusion* 60.1 (Oct. 2019), p. 016001. ISSN: 0029-5515. DOI: 10.1088/1741-4326/AB423E. URL: https://iopscience.iop.org/article/10.1088/1741-4326/ab423e%20https://iopscience.iop.org/article/10.1088/1741-4326/ab423e/meta.

[3] Yanzeng Zhang, Sergei I. Krasheninnikov, Rebecca Masline, and Roman D. Smirnov. "Neutral impact on anomalous edge plasma transport and its correlation with divertor plasma detachment". In: *Nuclear Fusion* 60.10 (Sept. 2020), p. 106023. ISSN: 0029-5515. DOI: 10.1088/1741-4326/ABA9EC. URL: https://iopscience.iop.org/article/10.1088/1741-4326/aba9ec%20https://iopscience.iop.org/article/10.1088/1741-4326/aba9ec/meta.

[4] N Bisai, Santanu Banerjee, and Deepak Sangwan. "Modification of plasma flows in edge and SOL regions by influence of neutral gas". In: *Phys. Plasmas* 25 (2018), p. 102503. DOI: 10.1063/1.5046723. URL: https://doi.org/10.1063/1.5046723.

[5] A.S. Thrysøe, M. Løiten, J. Madsen, V. Naulin, A.H. Nielsen, and J.J. Rasmussen. "Plasma particle sources due to interactions with neutrals in a turbulent scrape-off layer of a toroidally confined plasma". In: *Physics of Plasmas* 25.3 (2018). ISSN: 10897674. DOI: 10.1063/1.5019662.

[6] D A Russell, J R Myra, and D P Stotler. "A reduced model of neutral-plasma interactions in the edge and scrape-off-layer: Verification comparisons with kinetic Monte Carlo simulations". In: *Phys. Plasmas* 26 (2019), p. 22304. DOI: 10.1063/1.5081670. URL: https://doi.org/10.1063/1.5081670.

[7] G Avdeeva, V Naulin, A H Nielsen,) A H Nielsen, J Juul Rasmussen, and A S Thrysøe. "Influence of injection parameters on fueling efficiency of supersonic molecular beam injection into turbulent fusion plasmas". In: *Phys. Plasmas* 27 (2020), p. 62515. DOI: 10.1063/5.0002858. URL: https://doi.org/10.1063/5.0002858.

[8] D. Galassi, H. Reimerdes, C. Theiler, M. Wensing, H. Bufferand, G. Ciraolo, P. Innocente, Y. Marandet, and P. Tamain. "Numerical investigation of optimal divertor gas baffle closure on TCV". In: *Plasma Physics and Controlled Fusion* 62.11 (Sept. 2020), p. 115009. ISSN: 0741-3335. DOI: 10.1088/1361-6587/ABB24F. URL: https://iopscience.iop.org/article/10.1088/1361-6587/abb24f%20https://iopscience.iop.org/article/10.1088/1361-6587/abb24f/meta.

[9] A. Coroado and P. Ricci. "A self-consistent multi-component model of plasma turbulence and kinetic neutral dynamics for the simulation of the tokamak boundary". In: (Oct. 2021). URL: https://arxiv.org/abs/2110.13335v1.

[10] A Coroado and P Ricci. "Moving toward mass-conserving simulations of plasma turbulence and kinetic neutrals in the tokamak boundary with the GBS code". In: *Phys. Plasmas* 28 (2021), p. 22310. DOI: 10.1063/5.0027977. URL: https://doi.org/10.1063/5.0027977.

[11] D. A. Russell, J. R. Myra, F. Militello, and D. Moulton. "Reduced-model scrape-off layer turbulence (nSOLT) simulations comparing three fueling scenarios". In: *Physics of Plasmas* 28.9 (Sept. 2021), p. 092305. ISSN: 1070-664X. DOI: 10.1063/5.0060524. URL: https://aip.scitation.org/doi/abs/10.1063/5.0060524.

[12] W. Zholobenko, A. Stegmeir, M. Griener, G.D. Conway, T. Body, D. Coster, F. Jenko, and the ASDEX Upgrade Team. "The role of neutral gas in validated global edge turbulence simulations". In: *Nuclear Fusion* 61.11 (Oct. 2021), p. 116015. ISSN: 0029-5515. DOI: 10.1088/1741-4326/AC1E61. URL: https://iopscience.iop.org/article/10.1088/1741-4326/ac1e61%20https://iopscience.iop.org/article/10.1088/1741-4326/ac1e61/meta.

[13] S. I. Krasheninnikov, A. S. Kukushkin, and A. A. Pshenov. "Divertor plasma detachment". In: *Physics of Plasmas* 23.5 (May 2016), p. 055602. ISSN: 1070-664X. DOI: 10.1063/1.4948273. URL: https://aip.scitation.org/doi/abs/10.1063/1.4948273.

[14] A. W. Leonard. "Plasma detachment in divertor tokamaks". In: *Plasma Physics and Controlled Fusion* 60.4 (Feb. 2018), p. 044001. ISSN: 0741-3335. DOI: 10.1088/1361-6587/AAA7A9. URL: https://iopscience.iop.org/article/10.1088/1361-6587/aaa7a9%20https://iopscience.iop.org/article/10.1088/1361-6587/aaa7a9/meta.

[15] C. Theiler, B. Lipschultz, J. Harrison, B. Labit, H. Reimerdes, C. Tsui, W. A.J. Vijvers, J. A. Boedo, B. P. Duval, S. Elmore, et al. "Results from recent detachment experiments in alternative divertor configurations on TCV". In: *Nuclear Fusion* 57.7 (Mar. 2017), p. 072008. ISSN: 0029-5515. DOI: 10.1088/1741-4326/AA5FB7. URL: https://iopscience.iop.org/article/10.1088/1741-4326/aa5fb7%20https://iopscience.iop.org/article/10.1088/1741-4326/aa5fb7/meta.

[16] B. LaBombard, M. V. Umansky, R. L. Boivin, J. A. Goetz, J. Hughes, B. Lipschultz, D. Mossessian, C. S. Pitcher, and J. L. Terry. "Cross-field plasma transport and main-chamber recycling in diverted plasmas on Alcator C-Mod". In: *Nuclear Fusion* 40.12 (Dec. 2000), p. 2041. ISSN: 0029-5515. DOI: 10.1088/0029-5515/40/12/308. URL: https://iopscience.iop.org/article/10.1088/0029-5515/40/12/308%20https://iopscience.iop.org/article/10.1088/0029-5515/40/12/308/meta.

[17] D. L. Rudakov, J. A. Boedo, R. A. Moyer, P. C. Stangeby, J. G. Watkins, D. G. Whyte, L. Zeng, N. H. Brooks, R. P. Doerner, T. E. Evans, et al. "Far SOL transport and main wall plasma interaction in DIII-D". In: *Nuclear Fusion* 45.12 (Nov. 2005), p. 1589. ISSN: 0029-5515. DOI: 10.1088/0029-5515/45/12/014. URL: https://iopscience.iop.org/article/10.1088/0029-5515/45/12/014%20https://iopscience.iop.org/article/10.1088/0029-5515/45/12/014/meta.

[18] D. Carralero, H. W. Müller, M. Groth, M. Komm, J. Adamek, G. Birkenmeier, M. Brix, F. Janky, P. Hacek, S. Marsen, et al. "Implications of high density operation on SOL transport: A multimachine investigation". In: *Journal of Nuclear Materials* 463 (Aug. 2015), pp. 123–127. ISSN: 0022-3115. DOI: 10.1016/J.JNUCMAT.2014.10.019.

[19] D. Carralero, M. Siccinio, M. Komm, S.A. Artene, F.A. D'Isa, J. Adamek, L. Aho-Mantila, G. Birkenmeier, M. Brix, G. Fuchert, et al. "Recent progress towards a quantitative description of filamentary SOL transport". In: *Nuclear Fusion* 57.5 (May 2017), p. 056044. ISSN: 0029-5515. DOI: 10.1088/1741-4326/aa64b3. URL: http://stacks.iop.org/0029-5515/57/i=5/a=056044?key=crossref.0c6f1ef7d4e07bb4478a455b50a0b539.

[20] A. Wynn, B. Lipschultz, I. Cziegler, J. Harrison, A. Jaervinen, G. F. Matthews, J. Schmitz, B. Tal, M. Brix, C. Guillemaut, et al. "Investigation into the formation of the scrape-off layer density shoulder in JET ITER-like wall L-mode and H-mode plasmas". In: *Nuclear Fusion* 58.5 (Mar. 2018), p. 056001. ISSN: 0029-5515. DOI: 10.1088/1741-4326/AAAD78. URL: https://iopscience.iop.org/article/10.1088/1741-4326/aaad78%20https://iopscience.iop.org/article/10.1088/1741-4326/aaad78/meta.

[21] S. I. Braginskii, Braginskii, and S. I. "Transport Processes in a Plasma". In: *RvPP* 1 (1965), p. 205. URL: https://ui.adsabs.harvard.edu/abs/1965RvPP....1..205B/abstract.

[22] J D Hey, C C Chu, Ph Mertens, S Brezinsek, and B Unterberg. "Atomic collision processes with ions at the edge of magnetically confined fusion plasmas". In: *Journal of Physics B: Atomic, Molecular and Optical Physics* 37.12 (June 2004), pp. 2543–2567. ISSN: 0953-4075. DOI: 10.1088/0953-4075/37/12/010. URL: http://stacks.iop.org/0953-4075/37/i=12/a=010?key=crossref.c0382e761d3c2caf7c1335e72af9b10a.

[23] J D Hey, C C Chu, and Ph Mertens. "On corrections to spectroscopically measured Franck–Condon energies arising from motion of the parent molecules and from ion collisions in fusion plasmas: relevant time scales for atomic velocity distributions". In: *Journal of Physics B: Atomic, Molecular and Optical Physics* 38.19 (Oct. 2005), pp. 3517–3534. ISSN: 0953-4075. DOI: 10.1088/0953-4075/38/19/005. URL: http://stacks.iop.org/0953-4075/38/i=19/a=005?key=crossref.0c7b517fe0e7e290530951c93e606c6b.

[24] Olivier Izacard. "Generalized fluid theory including non-Maxwellian kinetic effects". In: *Journal of Plasma Physics* 83.2 (Apr. 2017), p. 595830201. ISSN: 0022-3778. DOI: 10.1017/S0022377817000150. URL: https://www.cambridge.org/core/product/identifier/S0022377817000150/type/journal_article.

[25] D. S. Oliveira and R. M.O. Galvão. "Transport equations in magnetized plasmas for non-Maxwellian distribution functions". In: *Physics of Plasmas* 25.10 (Oct. 2018), p. 102308. ISSN: 1070-664X. DOI: 10.1063/1.5049237. URL: https://aip.scitation.org/doi/abs/10.1063/1.5049237.

[26] A. Poulsen, J. Juul Rasmussen, M. Wiesenberger, and V. Naulin. "Collisional multispecies drift fluid model". In: *Physics of Plasmas* 27.3 (Mar. 2020), p. 032305. ISSN: 1070-664X. DOI: 10.1063/1.5140522. URL: https://aip-scitation-org.proxy.findit.dtu.dk/doi/abs/10.1063/1.5140522.

[27] S. H. Müller, C. Holland, G. R. Tynan, J. H. Yu, and V. Naulin. "Source formulation for electron-impact ionization for fluid plasma simulations". In: *Plasma Physics and Controlled Fusion* 51.10 (2009). ISSN: 07413335. DOI: 10.1088/0741-3335/51/10/105014.

[28] E. T. Meier and U. Shumlak. "A general nonlinear fluid model for reacting plasma-neutral mixtures". In: *Physics of Plasmas* 19.7 (July 2012), p. 072508. ISSN: 1070-664X. DOI: 10.1063/1.4736975. URL: https://aip.scitation.org/doi/abs/10.1063/1.4736975.

[29] L.D. Landau. "Kinetic equation for the Coulomb effect". In: *Phys. Z. Sowjetunion* 10.154 (1936).

[30] Ratko K. Janev, William D. Langer, Douglass E. Post, and Kenneth Evans. "Elementary Processes in Hydrogen-Helium Plasmas". In: *Elementary Processes in Hydrogen-Helium Plasmas* (1987). DOI: 10.1007/978-3-642-71935-6.

[31] V M Zhdanov. "Transport Processes in Multicomponent Plasma". In: *Plasma Physics and Controlled Fusion* 44.10 (Oct. 2002), pp. 2283–2283. ISSN: 0741-3335. DOI: 10.1088/0741-3335/44/10/701.

[32] M Wiesenberger and M Held. "Angular momentum and rotational energy of mean flows in toroidal magnetic fields". In: *Nuclear Fusion* 60.9 (Aug. 2020), p. 096018. ISSN: 0029-5515. DOI: 10.1088/1741-4326/AB9FA8. URL: https://iopscience.iop.org/article/10.1088/1741-4326/ab9fa8%20https://iopscience.iop.org/article/10.1088/1741-4326/ab9fa8/meta.

[33] R. Gerrú, M. Wiesenberger, M. Held, A. H. Nielsen, V. Naulin, J. J. Rasmussen, and H. Järleblad. "Conservation of currents in reduced full-F electromagnetic kinetic and fluid models". In: *Plasma Physics and Controlled Fusion* 64.5 (Mar. 2022), p. 054005. ISSN: 0741-3335. DOI: 10.1088/1361-6587/AC55F6. URL: https://iopscience.iop.org/article/10.1088/1361-6587/ac55f6%20https://iopscience.iop.org/article/10.1088/1361-6587/ac55f6/meta.

[34] Matthias Wiesenberger, Lukas Einkemmer, Markus Held, Albert Gutierrez-Milla, Xavier Sáez, and Roman Iakymchuk. "Reproducibility, accuracy and performance of the Feltor code and library on parallel computer architectures". In: *Computer Physics Communications* 238 (May 2019), pp. 145–156. ISSN: 0010-4655. DOI: 10.1016/J.CPC.2018.12.006.

[35] Jeppe Olsen, Jens Madsen, Anders Henry Nielsen, Jens Juul Rasmussen, and Volker Naulin. "Temperature dynamics and velocity scaling laws for interchange driven, warm ion plasma filaments". In: *Plasma Physics and Controlled Fusion* 58.4 (Feb. 2016), p. 044011. ISSN: 0741-3335. DOI: 10.1088/0741-3335/58/4/044011. URL: https://iopscience.iop.org/article/10.1088/0741-3335/58/4/044011%20https://iopscience.iop.org/article/10.1088/0741-3335/58/4/044011/meta.

[36] A. S. Thrysøe, V. Naulin, A. H. Nielsen, and J. Juul Rasmussen. "Dynamics of seeded blobs under the influence of inelastic neutral interactions". In: *Physics of Plasmas* 27.5 (May 2020), p. 052302. ISSN: 1070-664X. DOI: 10.1063/5.0003262. URL: https://aip.scitation.org/doi/abs/10.1063/5.0003262.

[37] M. Held, M. Wiesenberger, J. Madsen, and A. Kendl. "The influence of temperature dynamics and dynamic finite ion Larmor radius effects on seeded high amplitude plasma blobs". In: *Nuclear Fusion* 56.12 (2016). ISSN: 17414326. DOI: 10.1088/0029-5515/56/12/126005.

[38] O. E. Garcia, N. H. Bian, V. Naulin, A. H. Nielsen, and J. Juul Rasmussen. "Mechanism and scaling for convection of isolated structures in nonuniformly magnetized plasmas". In: *Physics of Plasmas* 12.9 (Sept. 2005), p. 090701. ISSN: 1070-664X. DOI: 10.1063/1.2044487. URL: https://aip.scitation.org/doi/abs/10.1063/1.2044487.